Semiconductor Physics, Quantum Electronics & Optoelectronics, 2021. V. 24, No 3. P. 341-347.

Optoelectronics and optoelectronic devices

Numerical simulation of perovskite solar cell with different material as electron transport layer using SCAPS-1D software

K. Bhavsar[1], P.B. Lapsiwala[2]

[1]*VPMP Polytechnic, LDRP campus, Gandhinagar,*
[2]*Sarvajanik College of Engineering and Technology, Surat Gujarat, India*
Corresponding author phone: 9925140518; e-mail: bhavsarkinjal26@gmail.com

Abstract. Perovskite solar cells have become a hot topic in the solar energy device area due to high efficiency and low cost photovoltaic technology. However, their function is limited by expensive hole transport material (HTM) and high temperature process electron transport material (ETM) layer is common device structure. Numerical simulation is a crucial technique in deeply understanding the operational mechanisms of solar cells and structure optimization for different devices. In this paper, device modelling for different perovskite solar cell has been performed for different ETM layer, namely: TiO_2, ZnO, SnO_2, PCBM (phenyl-C61-butyric acid methyl ester), CdZnS, C_{60}, IGZO (indium gallium zinc oxide), WS_2 and CdS and effect of band gap upon the power conversion efficiency of device as well as effect of absorber thickness have been examined. The SCAPS 1D (Solar Cell Capacitance Simulator) has been a tool used for numerical simulation of these devices.

Keywords: perovskite, solar cell, simulation, SCAPS-1D, power conversion efficiency, hole transport material, electron transport material.

https://doi.org/10.15407/spqeo24.03.341
PACS 88.40.hj, 88.40.hm, 88.40.jr

Manuscript received 25.12.20; revised version received 23.06.21; accepted for publication 18.08.21; published online 26.08.21.

1. Introduction

Perovskite solar cells (PSCs) represent an emerging photovoltaic technology due to their efficiency increased substantially from 3.8% efficiency recorded in 2009 [1] to 22.7% in 2017 [2] and about 27.3% in 2018 [3], which is still rising with pace. Fig. 1 shows the planer structure of perovskite solar cells. It consists of an electron transporting layer (ETL), absorbing layer and hole transporting layer (HTL). The absorbing layer constitutes of perovskite material and as inorganic HTMs include NiO, Cul, Cu_2O and CuSCN, whereas organic HTLs are spiro-MeOTAD, P_3HT, PTAA, PEDOT:PSS *etc*. and various ETLs are TiO_2, ZnO, SnO_2, PCBM (phenyl-C61-butyric acid methyl ester), CdZnS, C_{60}, IGZO (indium gallium zinc oxide), WS_2, CdS *etc*. Solar cell performance depends on its layers. G.A. Casas [4] proposed effects of using five different materials as HTL in perovskite solar cells have been analyzed and find out that the efficiency close to 28% has been obtained for Cu_2O/perovskite/TiO_2 solar cell.

In this work, different materials were studied for possible ETL like TiO_2, ZnO, SnO_2, PCBM, CdZnS, C_{60} (buckminsterfullerene), IGZO (indium gallium zinc oxide), WS_2 and CdS. The studies have been carried out by means of computer simulation. These materials have different mobilities (μ_n and μ_p), electron affinities (χ_e), band gap energies (E_g) and defect densities (N_t) due to these parameters alignments between the valence bands of both ETL and perovskite layer are different. Then performance parameters like open circuit voltage (V_{oc}), short circuit current (I_{sc}), fill factor (FF) and power conversion efficiency (PCE) change.

2. Materials and methods

2.1. Device structure and modelling

The perovskite ($CH_3NH_3PbI_3$) solar cell simulated in this work is shown in Fig. 1. It is one dimensional device with *n-i-p* planner structure. The *n*-region is ETL, the region is perovskite layer and *p*-region is HTL. When the cell is subjected to light, excitons (bound state of electron

© 2021, V. Lashkaryov Institute of Semiconductor Physics, National Academy of Sciences of Ukraine

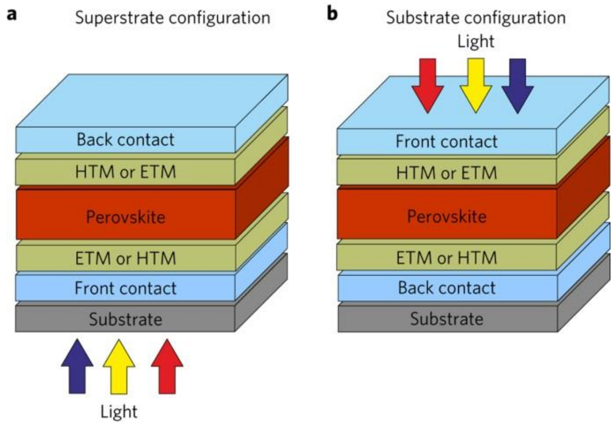

Fig. 1. General schematic structure for a perovskite solar cell, the sun is the illumination source [5]. ETL – electron transporting layer, HTL – hole transporting layer.

and hole) are mainly created in perovskite *i*-region. According to their diffusion length, they can reach the *n*(*p*)-region. At the *n/i* interface, the exciton is dissociated, and electron moves toward the *n*-layer, similarly at the input interface, exciton is dissociated and hole moves to the *p*-layer while remaining electron migrates to the *n*-layer. Dissociation of excitons as well as migration of electrons and holes are favoured by electrical field between the *n*- and *p*-layers.

Numerical simulation of planer perovskite solar cell were performed with one dimensional code SCAPS-1D (solar cells capacitance simulator), which is used to determine current density *vs* voltage characteristics, energy band diagram, quantum efficiencies/spectral response, functional parameters (open circuit voltage, total current density, fill factor, and power conversion efficiency), total recombination currents, AC quantities and electron/hole densities. This numerical program solves numerically the three basic semiconductor equations: the Poisson equation and continuity equations for holes and electrons (Raoui *et al.*, 2019 [6]; Jamil *et al.*, 2020 [7]).

The Poisson (1) and continuity equations for holes (2) and electrons (3) are as follows:

$$\frac{d}{dx}\left(\varepsilon(x)\frac{d\psi}{dx}\right)= \\ =q\left[p(x)-n(x)+N_D^+(x)-N_A^-(x)+p_t(x)-n_t(x)\right], \qquad (1)$$

$$\frac{1}{J}\frac{\partial J_p}{\partial x}+R_p(x)-G(x)=0\,, \qquad (2)$$

$$-\frac{1}{J}\frac{\partial J_n}{\partial x}+R_n(x)-G(x)=0\,. \qquad (3)$$

Here, ε is the permittivity, *q* – charge of electron, ψ – electrostatic potential and *n* – electrons' concentration, *p* – free hole concentration, n_t – trapped electron,

Table 1. Physical parameters for various ET layers [8].

Layer		ETL								
Parameters	**Symbol (Unit)**	**TiO_2**	**ZnO**	**PCBM**	**SnO_2**	**CdZnS**	**WS_2**	**C_{60}**	**IGZO**	**CdS**
Thickness	W (μm)	0.1	0.1	0.1	0.1	0.1	0.1	0.1	0.1	0.1
Band gap	E_g (eV)	3.2	3.3	2	3.5	3.2	1.8	1.7	3.05	2.4
Electron affinity	χ (eV)	3.9	4.1	3.9	4	4.2	3.95	3.9	4.16	4.5
Relative dielectric permittivity	ε_r	9	9	3.9	34.8	9.12	13.6	4.2	10	10
Effective density of states (DOS) in the conduction band	N_c (cm^{-3})	$1\cdot10^{19}$	$4\cdot10^{18}$	$2.5\cdot10^{21}$	$2.4\cdot10^{18}$	$1.5\cdot10^{18}$	$2.2\cdot10^{18}$	$8\cdot10^{19}$	$5\cdot10^{18}$	$2.2\cdot10^{18}$
Effective density of states (DOS) in the valence band	N_v (cm^{-3})	$1\cdot10^{19}$	$1\cdot10^{19}$	$2.5\cdot10^{21}$	$1.8\cdot10^{19}$	$1.8\cdot10^{19}$	$1.9\cdot10^{19}$	$8\cdot10^{19}$	$5\cdot10^{18}$	$1.9\cdot10^{19}$
Mobility of electrons	μ_e (cm^2·V^{-1}·s^{-1})	20	100	0.2	20	250	100	$8\cdot10^{-2}$	15	350
Mobility of holes	μ_h (cm^2·V^{-1}·s^{-1})	10	25	0.2	10	40	100	$3.5\cdot10^{-3}$	0.1	25
Acceptor density	N_A (cm^{-3})	0	0	0	0	0	0	0	0	0
Donor density	N_D (cm^{-3})	$1\cdot10^{16}$	$1\cdot10^{16}$	$1\cdot10^{16}$	$1\cdot10^{16}$	$1\cdot10^{16}$	$1\cdot10^{16}$	$1\cdot10^{16}$	$1\cdot10^{16}$	$1\cdot10^{16}$
Defect density	n_t (cm^{-3})	$1\cdot10^{14}$	$1\cdot10^{14}$	$1\cdot10^{14}$	$1\cdot10^{14}$	$1\cdot10^{14}$	$1\cdot10^{14}$	$1\cdot10^{14}$	$1\cdot10^{14}$	$1\cdot10^{14}$

Table 2. Physical parameters for absorber [8] and HT layer [3].

Layer		Perovskite [7]	HTL [3]
Parameters	**Symbol (Unit)**	$CH_3NH_3PbI_3$	Cu_2O
Thickness	W (μm)	0.6	0.4
Band gap	E_g (eV)	1.55	2.17
Electron affinity	χ (eV)	3.9	3.2
Relative dielectric permittivity	ε_r	32	6.6
Effective density of states (DOS) in the conduction band	N_c (cm^{-3})	$2.8\cdot10^{18}$	$2.50\cdot10^{20}$
Effective density of states (DOS) in the valence band	N_v (cm^{-3})	$3.9\cdot10^{18}$	$2.50\cdot10^{20}$
Mobility of electrons	μ_e (cm$^2\cdot$V$^{-1}\cdot$s^{-1})	11.8	80
Mobility of holes	μ_h (cm$^2\cdot$V$^{-1}\cdot$s^{-1})	11.8	80
Acceptor density	N_A (cm^{-3})	$1\cdot10^{13}$	$3\cdot10^{18}$
Donor density	N_D (cm^{-3})	$1\cdot10^{13}$	0
Defect density	n_t (cm^{-3})	$3\cdot10^{14}$	$1\cdot10^{15}$

Here, N_c and N_v are the effective density of states (DOS) in the conduction and valence bands, respectively, μ_h and μ_e – hole and electron mobilities, respectively, ε_r is the relative permittivity, and N_A and N_D are acceptor and donor impurity concentrations, respectively.

Table 3. Performance of solar cell obtained from simulations for each ETL material (according to ref. [8]).

Device structure	V_{oc} (V)		J_{sc} (mA/cm^2)		FF		PCE (%)	
	[8]	This work	[8]	This work	[8]	This work	[8]	This work
ZnO/$MAPbI_3$/Spiro-MeOTAD	1.01	1.07	26.79	24.38	82.89	82.64	22.37	21.73
SnO_2/$MAPbI_3$/Spiro-MeOTAD	1.00	1.05	26.66	24.41	82.59	82.58	22.13	21.35
TiO_2/$MAPbI_3$/Spiro-MeOTAD	1.00	1.05	26.76	24.39	82.66	82.99	22.24	21.37
CdZnS/$MAPbI_3$/Spiro-MeOTAD	0.99	1.08	26.78	24.37	83.19	78.77	22.25	20.08
IGZO/$MAPbI_3$/Spiro-MeOTAD	0.96	1.08	26.36	24.33	82.35	79.02	20.83	20.82
WS_2/$MAPbI_3$/Spiro-MeOTAD	1.00	1.05	26.40	24.50	83.76	81.55	22.11	21.07
PCBM/$MAPbI_3$/Spiro-MeOTAD	0.94	1.06	26.38	24.05	82.48	77.48	20.34	19.94
C_{60}/$MAPbI_3$/Spiro-MeOTAD	0.92	1.05	26.25	23.88	69.99	73.03	16.95	16.73
CdS/$MAPbI_3$/Spiro-MeOTAD	0.71	0.78	26.34	24.28	77.91	75.82	14.64	14.03

Table 4. Performance of solar cell obtained from simulations for each ETL material (proposed $MAPbI_3$ based *n-i-p* structures).

Device structure	V_{oc}, V	J_{sc}, mA/cm^2	FF	PCE, %
ZnO/$MAPbI_3$/Cu_2O	1.11	24.49	84.85	23.21
SnO_2/$MAPbI_3$/Cu_2O	1.10	24.49	83.18	22.48
TiO_2/$MAPbI_3$/Cu_2O	1.10	24.49	83.56	22.54
CdZnS/$MAPbI_3$/Cu_2O	1.12	24.49	82.86	22.74
IGZO/$MAPbI_3$/Cu_2O	1.12	24.44	82.88	22.69
WS_2/$MAPbI_3$/Cu_2O	1.09	24.57	81.46	22.05
PCBM/$MAPbI_3$/Cu_2O	1.10	24.13	78.14	20.85
C_{60}/$MAPbI_3$/Cu_2O	1.09	23.80	72.16	18.83
CdS/$MAPbI_3$/Cu_2O	1.12	24.42	58.94	16.19

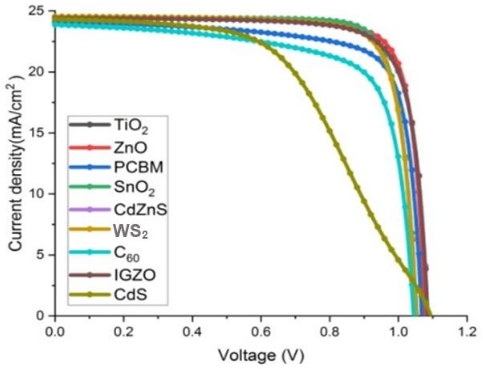

Fig. 2. Effect of different ETL layer on current density *vs* voltage characteristics. (Color online.)

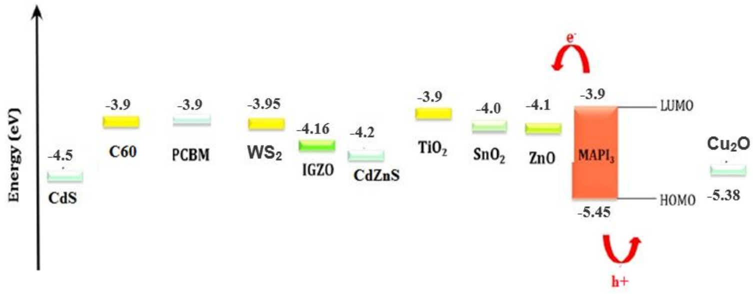

Fig. 3. Bands alignment between ETL, perovskite and HTL [9].

p_t – trapped hole, N_D^+ – ionized donor like doping and N_A^- – ionized acceptor like doping concentrations, $R_n(x)$, $R_p(x)$ are electrons and holes recombination rates, $G(x)$ is the generation rate, J_n and J_p are the electron and hole current densities, respectively.

The device modelling in this work was performed by SCAPS-1D software. In this approach, perovskite solar cells are simulated with three input layers, where *n*-type TiO_2, ZnO, SnO_2, PCBM, CdZnS, C_{60}, IGZO, WS_2 and CdS are used separately in order to compare their performance as ETL, perovskite is used as an absorbing layer, and *p*-type Cu_2O is used as HTL. Here, carbon is used as the back contact, and fluorine doped tin oxide (FTO) – as the front contact. For simulation under illumination condition standard AM1.5G spectrum (1000 W/m^2, T = 300 K) was used.

For simulation, physical parameters used for different ETL layers are given in Table 1, while those for the absorbing ($CH_3NH_3PbI_3$) and HT layers are given in Table 2.

3. Results and discussion

3.1. Comparisons analysis of different ETLs and their performance

According to Khattak *et al*. [7], the effect of band gap width and electron affinity of ETL on solar cell performance having the device structure ETL/MAPbI$_3$/Spiro-MeOTAD for different ETLs having the same donor doping concentration and thickness given in Table 3 from these results indicates that each ETL has its own effect on parameters, namely: short circuit current, open circuit voltage, fill factor and conversion efficiency. This is caused by different band structures of ETL, which can be offered when forming the junction with the absorbing layer.

The result of PCE calculated for various ETL materials and keeping fixed the HT and perovskite layers are summarized in Table 4.

In this paper, Cu_2O is used as HTL material, because according to Casas *et al*. [4] this material gives the maximum efficiency. In all these ETLs have the same donor doping concentration $1\cdot10^{16}\,cm^{-3}$, and the thickness value is 0.1 µm as optimized by Khattak *et al.* [8]. From this result, it is observed that each ETL has its own effect on different performance parameters, namely: short circuit current (J_{sc}), open circuit voltage (V_{oc}), fill factor and PCE of ETL (*n*-type)/perovskite ($CH_3NH_3PbI_3$)/HTL (Cu_2O, *p*-type) device structure. The effect of different ETLs on performance parameters is described in Table 4, and the current density *vs* voltage characteristics is demonstrated in Fig. 2. According to these results, we find out that as ETL ZnO material structure gives maximum PCE (23.21%). This happens because of different band structures that ETL can offer when forming a junction with the absorbing layer. The type of band structure that ETL can form with the absorbing layer is shown in Fig. 3.

The best efficiency is noticed for ZnO, SnO_2, TiO_2, CdZnS, IGZO and WS_2 above 20%. This is caused by adequate bands' alignment between the conduction band and LUMO (Lowest Unoccupied Molecular Orbital) of perovskite according to Figs 3 and 4, and also consider that some of their input parameters seem to be similar, but it is also influenced by the mobility of electrons and defect density.

3.2. Effect of variation in the absorber thickness

The effect of absorber thickness from 0.2 to 4.0 µm is shown in Fig. 5 for the required parameters: short circuit current (J_{sc}), open circuit voltage (V_{oc}), fill factor (FF) and PCE. Here, V_{oc} decreases from 1.16 down to 1.02 V, FF changes from 86.00 to 73.45%, J_{sc} increases up to 1.5-µm thickness, and after that the constant value is obtained and PCE (23.21%) reaches its maximum at the 0.6-µm absorber thickness. So, it is conformed from this data of 0.6-µm thickness that the absorbing layer has better performance and higher PCE (23.21%) with FF (84.85%) and J_{sc} (24.49 mA/cm^2) parameters' values.

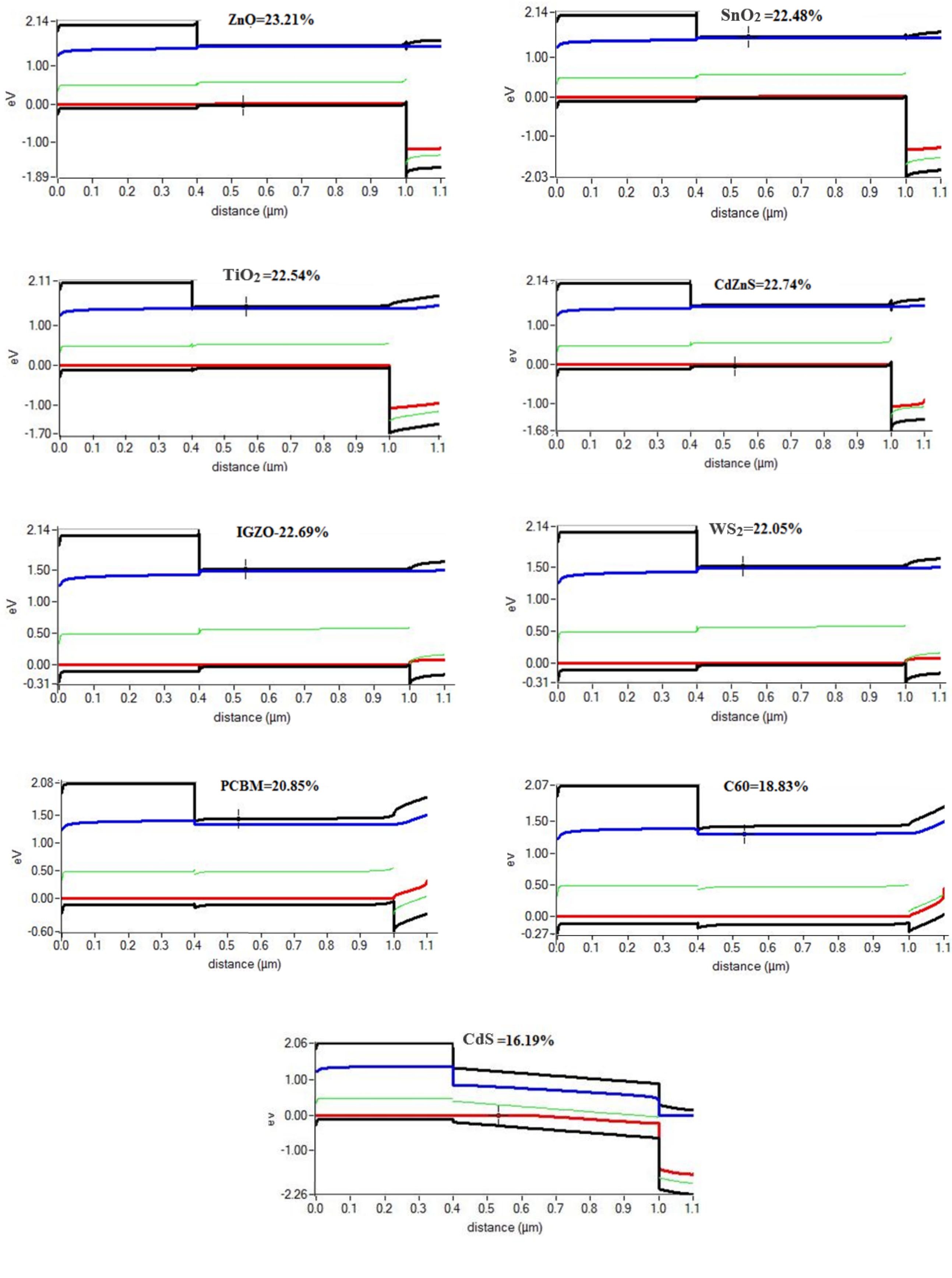

Fig. 4. Band diagram of ETL with the absorbing layer.

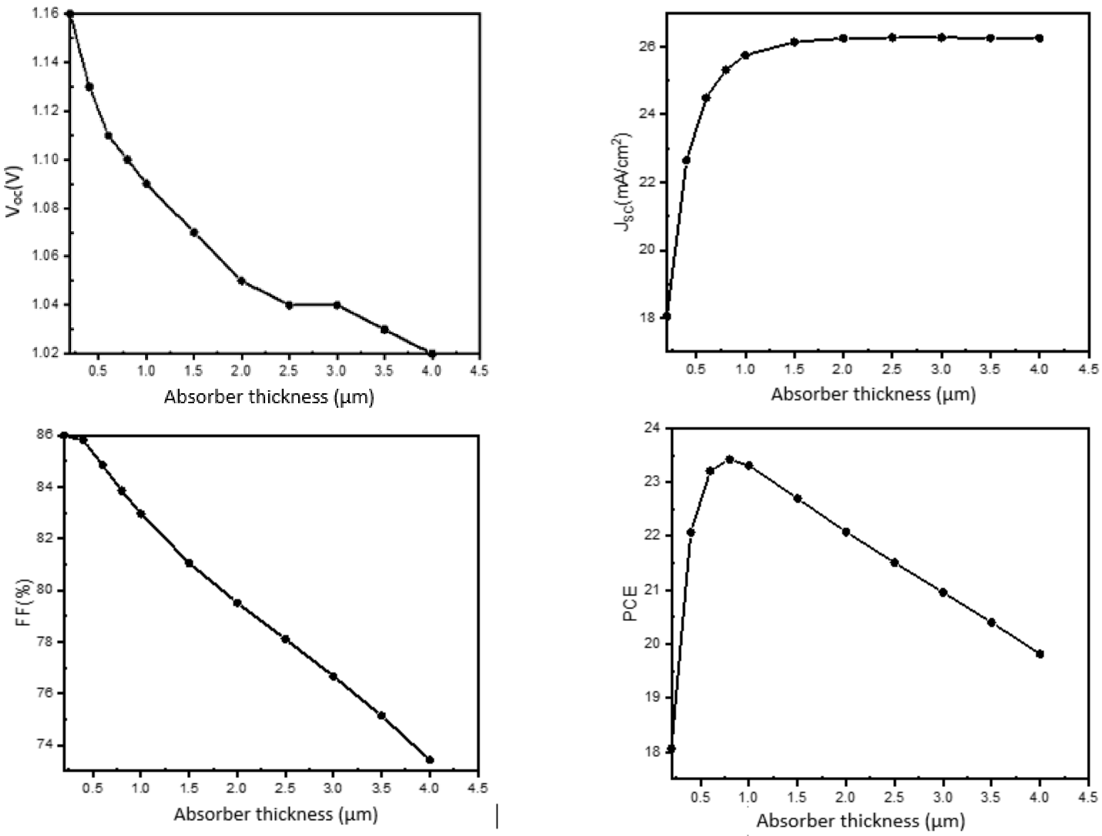

Fig. 5. Variation in absorber thickness with respect to performance parameters, keeping fixed ETL and HTL thicknesses.

4. Conclusions

In this work, detailed analysis has been performed for modelling the *n-i-p* structure for $CH_3NH_3PbI_3$ based perovskite solar cells. SCAPS-1D software was used for this modelling and nine different materials (TiO_2, ZnO, SnO_2, PCBM, CdZnS, C_{60}, IGZO, WS_2 and CdS) as electron transporting layer and Cu_2O as hole transport layer. The results obtained in this work show that most crucial effect on PCE is alignment between the maximum of valence band of ETL and perovskite materials which is directly related to band gap energy and electron affinity of each material. The band alignment is not only parameters that affect the better efficiency of cell but also mobility, which plays a crucial role between materials that have almost similar band alignment properties. The effect of variation in thickness of absorber on power conversion efficiency has been studied and optimized thickness found to be 0.6 µm with better PCE close to 23.21%.

References

1. Green M., Ho-Baillie A. & Snaith H. The emergence of perovskite solar cells. *Nature Photon*. 2014. **8**. P. 506–514. https://doi.org/10.1038/nphoton.2014.134.
2. Green M., Hishikawa Y., Dunlop E. *et al.* Solar cell efficiency tables (version 51). *Prog. Photovolt.* 2018. **26**, No 1. P. 3–12. https://doi.org/10.1002/pip.2978.
3. Osborne M. Oxford PV takes record perovskite tandem solar cell to 27.3% conversion efficiency. PVTECH, June 25, 2018.
4. Casas G.A., Cappelletti M.A., Cédola A.P. *et al.* Analysis of the power conversion efficiency of perovskite solar cells with different materials as Hole-Transport Layer by numerical simulations. *Superlattices and Microstructures.* 2017. **107**. P. 136–143. https://doi.org/10.1016/j.spmi.2017.04.007.
5. Fan F., Feurer T., Weiss T.P. *et al.* High-efficiency inverted semi-transparent planar perovskite solar cells in substrate configuration. *Nat. Energy.* 2017. **2**. P.16190. https://doi.org/10.1038/nenergy.2016.190.
6. Raoui Y., Ez-Zahraouy H., Tahiri N. *et al.* Performance analysis of $MAPbI_3$ based perovskite solar cells employing diverse charge selective contacts: Simulation study. *Sol. Energy.* 2019. **193**. P. 948–955. https://doi.org/10.1016/j.solener.2019.10.009.
7. Jamil M., Ali A., Mahmood K. *et al.* Numerical simulation of perovskite/$Cu_2Zn(Sn_{1-x}Ge_x)S_4$ interface to enhance the efficiency by valence band offset engineering. *J. Alloys Compd.* 2020. **821**. P. 153–221. https://doi.org/10.1016/j.jallcom.2019.153221.

8. Khattak Y.H., Baig F., Shuja A., Beg S., Soucase B.M. Numerical analysis guidelines for the design of efficient novel *nip* structures for perovskite solar cell. *Solar Energy*. 2020. **207**. P. 579–591. https://doi.org/10.1016/j.solener.2020.07.012.
9. Azri F., Meftah A., Sengouga N., Meftah A. Electron and hole transport layers optimization by numerical simulation of a perovskite solar cell. *Solar Energy*. 2019. **181**. P. 372–378. https://doi.org/10.1016/j.solener.2019.02.017.

Authors and CV

Kinjal Bhavsar received BE in Electronics & Communication from North Gujarat University in 2000. She completed her M.Tech in VLSI design from Nirma University of Technology, Ahmedabad in 2011. She is pursuing PhD from GTU, Ahmedabad. She worked as an academician university professor in the department of Electronics and Communication Engineering at VPMP Polytechnic, Gandhinagar from 2007. Her research interests are in semiconductor physics, optoelectronics, and VLSI design.
ORCID: https://orcid.org/0000-0002-8944-7364

Dr **Pranav Lapsiwala** born in Surat, Gujarat on 25th May 1980, received BE in Electronics & Communication from Veer Narmad South Gujarat University in 2002. He completed his MS in Telecommunication Network from University of Technology Sydney, Australia in year 2005. He awarded PhD in 2015 in Electronics Engineering from Rashtrasant Tukadoji Maharaj, Nagpur University. He is carrying over two decade of work experience with cover of technical consultancy of Engineering Projects and Product development with academic collaboration – Teaching and Learning Graduate School to PhD. Within technical consultancy, worked across RF – Optical Engineering Projects, Microwave CVD Projects for Diamond Industry. Since the recent decade, from August 2006, he worked as an academician university professor, in the department of Electronics and Communication Engineering at Sarvajanik College of Engineering & Technology, Gujarat, where he is presently holding the position of Associate Professor.

ORCID: https://orcid.org/0000-0002-3046-0601
E-mail: pranav.lapsiwala@scet.ac.in.

Чисельне моделювання сонячного елемента на основі перовскіту з різним матеріалом шару з електронною провідністю за допомогою програмного забезпечення SCAPS-1D

K. Bhavsar, P.B. Lapsiwala

Анотація. Сонячні елементи на основі перовскіту стали гарячою темою в області приладів сонячної енергетики завдяки високій ефективності та недорогій технології фотовольтаїки. Однак їх застосування обмежено високою вартістю матеріалу, що забезпечує діркову провідність, у той же час високотемпературний шар матеріалу з електронною провідністю є загальною структурою таких пристроїв. Чисельне моделювання є найважливішим методом для глибокого розуміння механізмів роботи сонячних елементів та оптимізації структури для різних пристроїв. У цій роботі проведено моделювання пристрою для різних перовскітних сонячних елементів для різних шарів із матеріалу з дірковою провідністю, а саме: TiO_2, ZnO, SnO_2, PCBM, CdZnS, C60, IGZO, WS_2 та CdS, та досліджено вплив ширини забороненої зони на ефективність перетворення енергії пристрою, а також вплив товщини поглинаючого шару. SCAPS 1D (імітатор ємності сонячних елементів) є інструментом, що використовується для чисельного моделювання цього пристрою.

Ключові слова: перовскіт, сонячний елемент, моделювання, SCAPS-1D, ефективність перетворення енергії, матеріал з електронною провідністю, матеріал з дірковою провідністю.